We are IntechOpen, the world's leading publisher of Open Access books Built by scientists, for scientists

4,800
Open access books available

122,000
International authors and editors

135M
Downloads

Our authors are among the

154
Countries delivered to

TOP 1%
most cited scientists

12.2%
Contributors from top 500 universities

CLARIVATE ANALYTICS BOOK CITATION INDEX INDEXED

WEB OF SCIENCE™

Selection of our books indexed in the Book Citation Index in Web of Science™ Core Collection (BKCI)

Interested in publishing with us?
Contact book.department@intechopen.com

Numbers displayed above are based on latest data collected.
For more information visit www.intechopen.com

Chapter 12

Numerical Simulation in Ulcer-Like Projection due to Type B Aortic Dissection with Complete Thrombosis Type

Futoshi Mori, Hiroshi Ohtake, Go Watanabe and Teruo Matsuzawa

Additional information is available at the end of the chapter

http://dx.doi.org/10.5772/52559

1. Introduction

The aging society has rapidly progressed worldwide and the mortality and morbidity rates of aortic diseases are increasing. In particular, aortic aneurysm and aortic dissection are serious disorders. These may be fatal if their diagnosis and treatment are delayed. In 2006, guideline for the diagnosis and treatment of aortic aneurysm and aortic dissection was established in Japan [1]. In 2010, a guideline for the diagnosis and management of patients with thoracic aortic diseasewas established in the United States[2]. These guidelines pay particular attention to the diagnosis and treatment of aortic diseases. We investigated the possibility of estimating time-dependent changes in these diseases using Computational Fluid Dynamics (CFD) simulation. This chapter describes the numerical simulations used for ulcer-like projections due to aortic dissections with complete thrombosis. By combining the results of CFD and diagnostic imaging, we can anticipate future improvements in diagnosis.

1.1. Definition and classifications of aortic dissection

A blood vessel wall comprises three layers: the intima (inner layer), the media (middle layer), and the adventitia (outer layer). The pathogenesis of an aortic dissection involves an intimal tear or damage to the aortic wall. This condition is characterized by the rapid development of an intimal flap that separates the true lumen from the false lumen [3]. Intimal flap tears are characteristic of communicating dissections. The communication of blood flow between the true lumen and the false lumen is through the entry part and the re-entry part of the tear. Figure 1 shows a schematic diagram of an aortic dissection [4].

The clinical pathological condition of an aortic dissection is classified according to three aspects: the region of dissection, blood flow in the false lumen, and the disease stage. Figure 2 shows the classifications of aortic dissections. Classifications according to the region of dissection are the Stanford [5] and DeBakey [6] classifications. The Stanford classification is divided into two types, A and B, depending on whether or not the ascending aorta is involved. The treatment methodsfor Stanford Type A (Type A) and Type B (Type B) are different based on the diagnosis of the aortic dissection. Type A requires emergency surgery, whereas Type B is generally treated by antihypertensive treatment that is regulated with medical therapy. The mortality rate for Type B is lower than that for Type A. However, one in four people with this disease die per year. The DeBakey classification is categorized as DeBakey I, II, and III. DeBakey I involves both the ascending and descending aortas, DeBakey II involves only the ascending aorta, and DeBakey III involves only the ascending aorta. In addition, aortic dissections can be classified based on blood flow in the false lumen. A dissection with patent proximal and patent distal re-entry tears in the absence of a thrombus is defined as a patent type. Dissections with a false lumen that is filled with thrombus and no longer communicates with the true lumen are defined as complete thrombosis type [7]. The complete thrombosis type is designated as intramural hematoma (IMH) in the United States and Europe [8]. Finally, the classifications according to the disease stage are categorized as acute if they occur within two weeks of the development of disease and chronic if they occur after that. As per recent trend in emergency medicine, the development of disease within 48 has been classified as a super-acute stage.

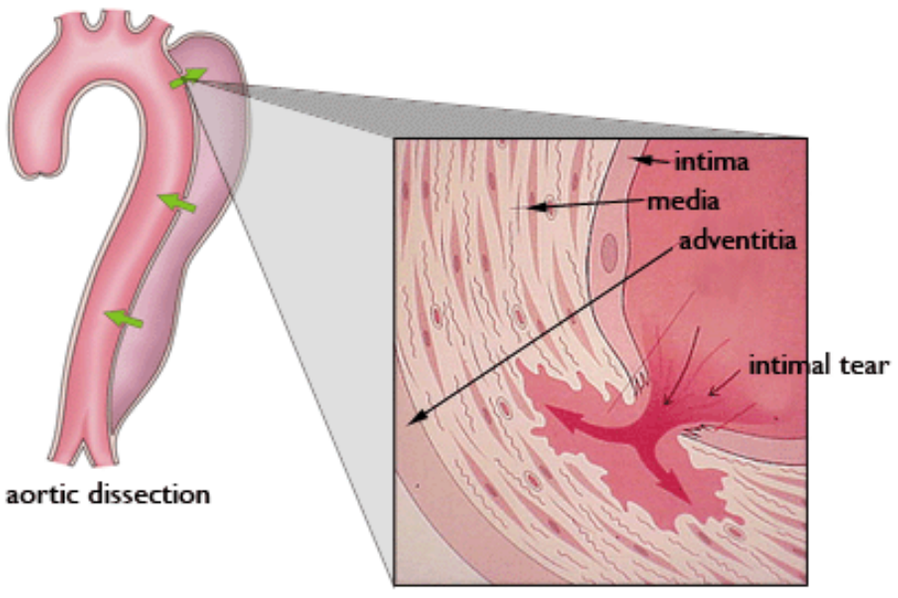

Figure 1. Schematic diagram of an aortic dissection [4].The pathogenesis of aortic dissection is an intimal tear or damage to the aortic wall.This condition is characterized by the rapid development of an intimal flap that separates the true lumen from the false lumen.

http://dx.doi.org/10.5772/52559

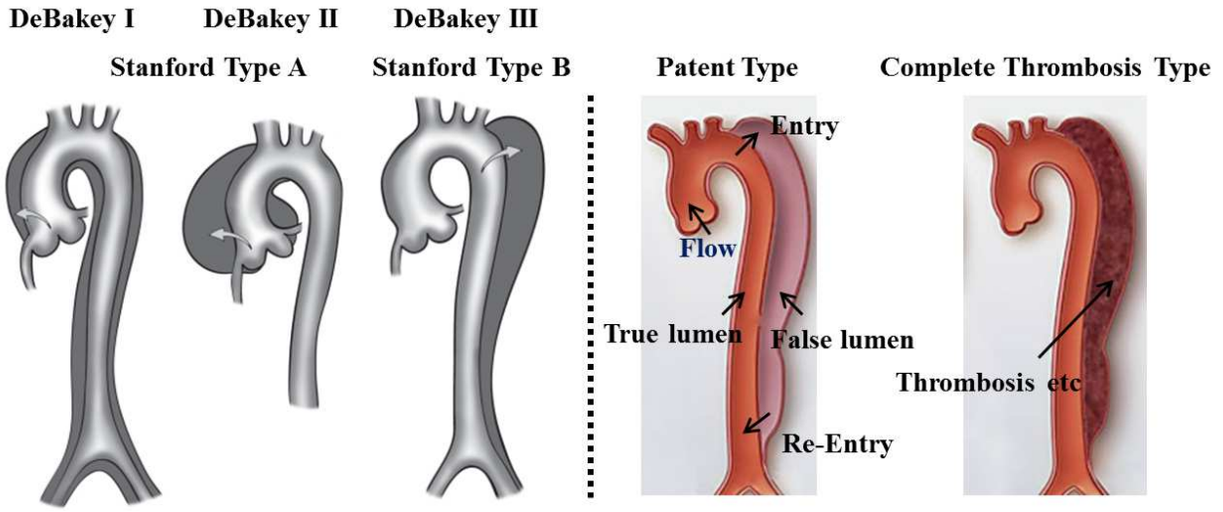

Figure 2. Classifications of aortic dissections. Based on regions of dissection: DeBakey and Stanford types (left) [9] the blood flow in the false lumen: Patent type and Complete Thrombosis type (right) [7]

1.2. Ulcer-like projection in aortic dissection

An ulcer-like projection (ULP) that occurs during the course of the complete thrombosis type [10, 11] and a penetrating atherosclerotic ulcer (PAU) due to an arteriosclerotic ulcer [12, 13] are conceptually different.ULP is an ulcerative projection image of the contrast medium that comparatively has a smooth outline and is a defect of the inner membrane continuous to the false lumen was condensed. Recently, ULP is treated as subtype (ULP type in aortic dissection) [1]. Moreover, PAU is a disease associated with bleeding and hematoma in the inner membrane. However, it is extremely difficult to clearly distinguish ULPs and PAUs in current medical diagnosis. This chapter describes ULPs.

An ULP is often detected with an improved the medical treatment imaging device such as the multi detector-row computed tomography (MDCT). A total of 170 patients admitted with acute Type B of the complete thrombosis type, 62 (36%) of these patients showed new ULP development [14]. Moreover, Kitai et al. retrospectively analyzed 38 consecutive patients who had a complete thrombosis type without an ULP. They underwent 64-row MDCT during the acute phase, and 71% of these patients were found to have intimal defects [15]. The presence of an intimal defects has been found to be a significant risk factor for evolution of IMH to an over dissection, rupture or aneurysmal dilation [16-18]. For Type A, Koshino et al. reported that ULPs developed after treatment [19]. For Type B, Tsai et al. reported that an ULP was discovered at a significant frequency for the complete thrombosis type [7]. It was clear that imaging diagnosis was an effective technique for detecting an ULP.

The survival rate of the patients who developed ULPs was higher than that of the patients who did not develop ULPs [14]. The presence or absence of ULP was a significant difference in the incidence of complications [20]. The kinds of complications were the aneurysm, aortic dissection and acute complication. Therefore, to prevent a residual ULP from forming an aneurysms and rupturing, postoperative angiography should be scheduled early after the

initial surgery. In those cases when an ULP is found, surgical treatment must be done as soon as possible. For the complete thrombosis type, presence or absence of an ULP becomes a diagnostic standard. A sample CT image with an ULP reportedly has a bad prognosis [14, 16, 21]. In such cases involving an ULP, the time-dependent changes in ULPs have been discussed, which involve expansion, invariability, reduction, and disappearance [22]. The reasons for time-dependent change in an ULP are thought to be due to various factors. The parts of the aorta where the expansion tendency for an ULP is strong are the ascending aorta, the aortic arch, and the proximal descending aorta [16]. These common points are places where the influence of hemodynamics is readily applied. Moreover, an ULP can become an aneurysm during this course. The complete thrombosis type is changed to a patent type based on an ULP that might rupture. Currently, the estimation by CFD simulation for the time-dependent change is performed. The next section describes about CFD simulation.

1.3. Computed fluid dynamics simulation

It has been established using Computational Fluid Dynamics (CFD) simulations that dynamic stress is a risk factor for time-dependent changes in blood vessel configuration [23]. The recent trend in bio-fluid research is to reconstruct the blood vessel of a patient with aneurysms from the medical images and examine the distributions of several parameters, such as velocity vectors, pressures and wall shear stress (WSS) [24, 25]. Low shear has been associated with aneurysm progression [26], thrombus formation [27], and artery wall rupture [28, 29]. Karmoniket al. showed that an occlusion ofthe re-entry part increased the pressure in the false lumen in an aortic dissection [30]. Watanabe et al. reported that in the case of a partial thrombosis type,there was an increased a risk of complications [31]. In the complete thrombosis type at the systolic phase, the pressure in the false lumen is higher than that in the true lumen. In the entry part, the change in distribution indicated an effect on the intima. Shimogonya et al. performed numerical simulations to examine the formation of an aneurysm [32]. In the following sections, we will examine these factors and, in particular, concentrate on the role of hemodynamics.

2. Reconstruction shape in aortic dissection with an ULP

2.1. Observations of medical images

Imaging diagnosis using computed tomography (CT), magnetic resonance imaging (MRI), and others has significantly advanced. Thus, an accurate, prompt diagnosis is possible because of these advances. Recently, MDCT has been used. The significance of CT images has increased in the diagnosis of aortic dissections. Targeted a ULP caused by aortic dissections were all diagnosed to be saccular aneurysms. The saccular aneurysm requires a surgical adjustment because it has a tendency to rupture even when it is small.

Our study included 2 patients (sex: males; ages:Case 1, 75 years old, and Case 2, 70 years old). Both had a type B complete thrombosis aortic dissection with an ULP. The locations of their ULPs were the descending aorta. There were diagnosed by a medical doctor and ULPs

http://dx.doi.org/10.5772/52559

showed tendencies for expansion. The period for obtaining images was approximately one month. This period included time points before the development of an ULP to immediately before the rupture of the ULP. These volunteers were treated within two weeks after an image was obtained immediately before rupture and they were recovering. Figure 3 shows the medical images of an ULP in an aortic dissection on vertical (left) and sagittal (right) views using contrast medium. By including the contrast medium, the brightness of blood flow region on the image was higher than the other parts. This ULP was caused by the aortic dissection of the complete thrombosis type. Thrombosis was present near the ULP. The format used for this image was Digital Imaging and Communications in Medicine (DICOM). DICOM is a standard for handling, storing, printing and transmitting information for medical images. Avizo v6.3 software (Visualization Sciences Group) was used to reconstruct the aortic dissection with an ULP model based on the DICOM images of these volunteers.

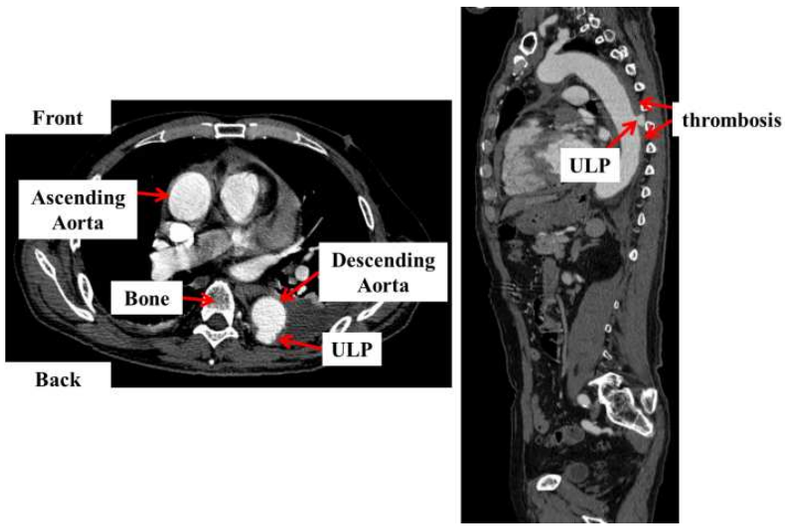

Figure 3. Ulcer-like projection in an aortic dissection of the complete thrombosis type on vertical (left) and sagittal (right) views. The location of the ULP is the descending aorta. This medical image includes a contrast medium.

2.2. Procedure of the reconstructed shape from the medical images

A realistic 3D model was reconstructed from 2D medical images using the procedure shown in figure 4. A DICOM file represents a slice of the body, as illustrated in figure3. We need to segment the blood flow region in order to generate volume data.A blood vessel region can be extracted manually by marking using Avizo v7.0.0 (VSG). The volume data are generated from the segmented part and the volume data are transferred to the stereo lithography (STL) format. STL format describes a raw, unstructured triangulated surface by a unit normal and vertices of the triangles using a 3D Cartesian coordinate system.However, the surface data that are obtained include triangle with bad aspect ratios. Thus, it is necessary to smooth the surface using Magics v9.54 (Materialize, JAPAN). A patient-specific aortic dissection with an ULP model in STL format was reconstructed from CT medical images, as illustrated in figure 4 (right).

The time-series reconstructed shape is illustrated in figure 5. The period of time-dependent change from the development of an ULP, designated Case 1A, to immediately after the rupture of the ULP, designated Case 1B, was about 1 month. In figure 5, the symbol X indicates ulceration of the artery. The symbol Y indicates that the artery is expanded, although the aneurysm was not located at this position according to the diagnosis.

A tetrahedral numerical mesh was generated using commercial software (Gambit 2.4.6, ANSYS, Inc., Canonsburg, PA).

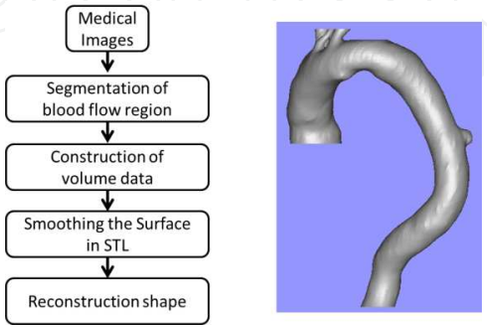

Figure 4. Procedure for reconstructing shape from medical images (left), and the reconstructed shape (right)

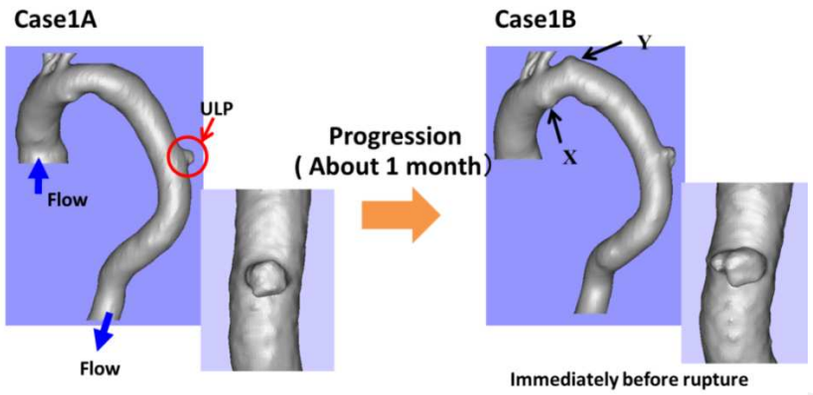

Figure 5. Time-series reconstructed shape of an aortic dissection with an ULP. The symbol X indicates ulceration of the artery and the symbol Y indicates that the artery is expanded although the aneurysm was not located at this position according to the diagnosis.

3. Numerical simulations of the time-dependent changes of an ULP in a Type B aortic dissection of the complete thrombosis type

3.1. Governing equations

This simulation calculated an unsteady-state solution. The governing equations were the following Navier-Stokes equation (1), and continuity equation (2):

http://dx.doi.org/10.5772/52559

$$\rho\left\{\frac{\partial\vec{u}}{\partial t}+(\vec{u}\cdot\nabla)\vec{u}\right\}=-\nabla p+\mu\nabla^2\vec{u} \tag{1}$$

$$\nabla\cdot\vec{u}=0 \tag{2}$$

where$\vec{u}=(u \quad v \quad w)$is a flow vector, ϱ=1.05 ×10^3 kg/m^3 is the density, p is the pressure and μ=3.5 ×10^3 N·s/m^2 is the viscosity.

We assumed the physical properties of blood. The maximum Reynolds number of the aorta at its maximum diameter in a human has been measured [33]. We assumed a Reynolds number of 6500, which is a mean value based on the literature. Blood flow was simplified as being isothermal, incompressible, and laminar Newtonian flow with a density of ϱ= 1.05 × 10^3 kg/$m^3$and a viscosity of μ= 3.5 ×10^3 N s/m^2. A k-ε model was used for turbulent flow because the flow structure of the aorta indicated that its blood flow became turbulent.

3.2. Calculation of boundary conditions

The boundary conditions used for the inlet, outlet, and blood vessel wall were as follow. The inlet boundary condition was set to the velocity profile, illustrated in figure 6 [34]. The outlet boundary condition was set to 0 Pa at the abdominal aorta. The boundary conditions for bifurcations that were at the innominate artery, the left common carotid artery, and the left subclavian artery in the upper side referred to the length from the inlet end to the outlet end and the balance of the flow rate and cross-section were set to 1:1. A no-slip condition was applied to the blood vessel wallas it was assumed to be rigid. Figure 7 illustrates the boundary conditions used in Case 1. Calculations using the finite volume method were made using a commercial solver (Fluent 6.3.26, Fluent Inc., NH). The results of similar trends were seen in Case 1 and Case 2. The results for Case 1 are shown in the following section.

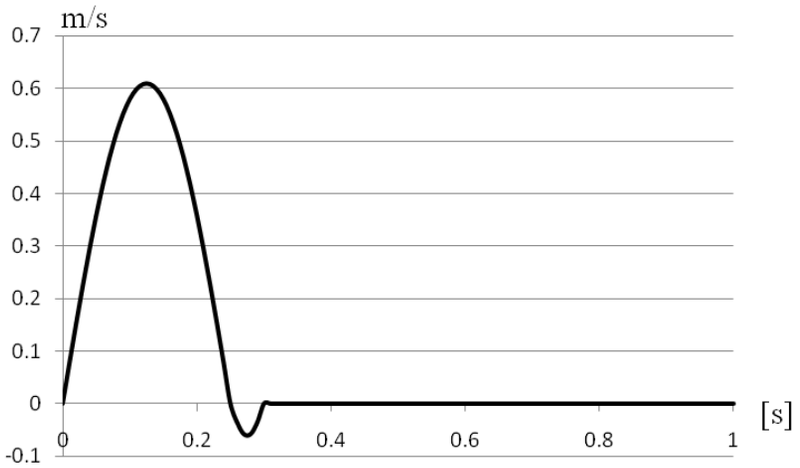

Figure 6. Velocity profile applied at the inlet end based on the literature [34]

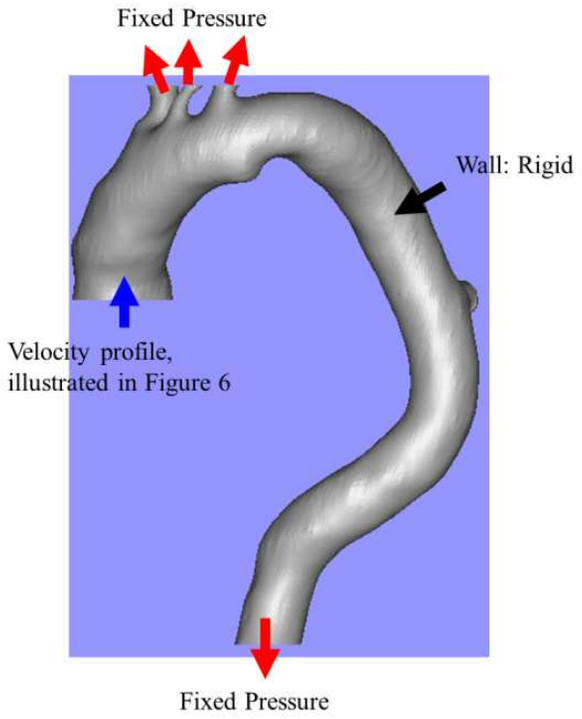

Figure 7. Boundary conditions: Inlet was set to the velocity profile in figure 6, outlet was set to a fixed pressure, and the wall was set to rigid, no-slip.

3.3. Simulation results

Figure 8 shows blood flow using the streamlines in each case at four time points (t=0.06, 0.12, 0.18, and 0.50). The flows in the aortic arch and descending aorta were faster than for Case 1B. Case 1B showed a tendency to expand and the volume of the configuration based on the time-dependent change was possibly increasing. The flow in the ULP was observed to be a vortex.

We examined the secondary flow in the ULP. During the systolic phase and excluding the adverse flow, the cross-sectional direction for the flow in the horizontal section was decided based on the flow direction in the vertical section proximal to the ULP. Figure 9 shows the secondary flow using the vectors in the ULP for Case 1A and Case 1B. The flow direction was flowing in the same direction compare to case 1A and case 1B. The flow entering from the bottom of the ULP had been outflowed from the top side after circling. In addition, the movement of the vortex core was observed using the line integral convolution (LIC) method, as illustrated in figure 10. The vortex core in the ULP moved from the outside to the inside with the passage of time. The trend for the vortex core track was consistent in each case. Therefore, there was a possibility for the ULP to expand further in Case 1B. In Case 1B, multiple vortices in the ULP were observed. Most ruptured aneurysm had complex flow patterns with multiple vortices [35, 36]. In contrast, most un-ruptured aneurysm had simple flow patterns with single vortices. Therefore, two points, which are the movements of the

http://dx.doi.org/10.5772/52559

vortex core and multiple vortices, can be estimated for the expansion of an ULP during the movement of its vortex core.

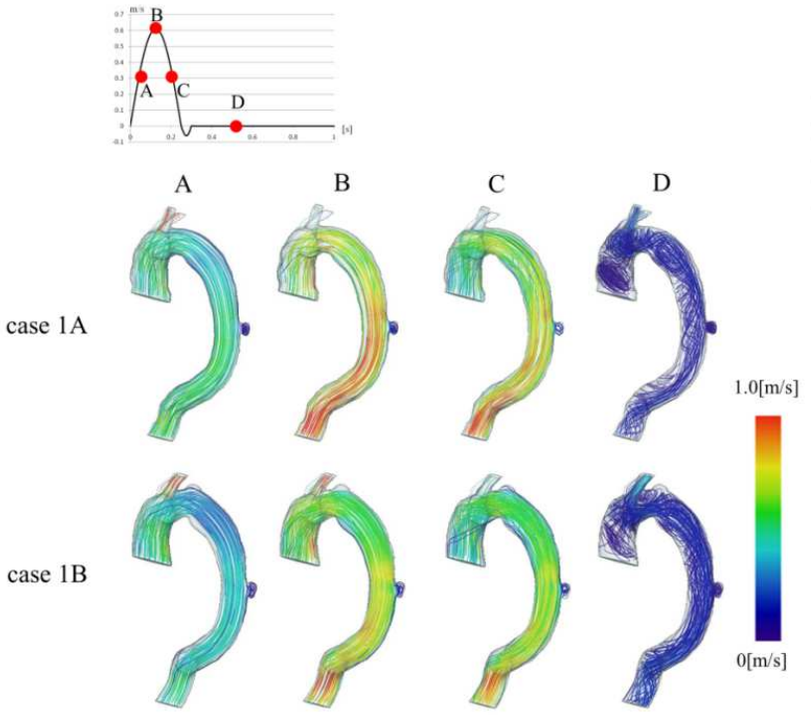

Figure 8. Flow using the streamlines in Case 1A (upper) and Case 1B (lower) at four time points (t=0.06, 0.12, 0.18, and 0.50). Blue indicates slow speed and red indicates high speed

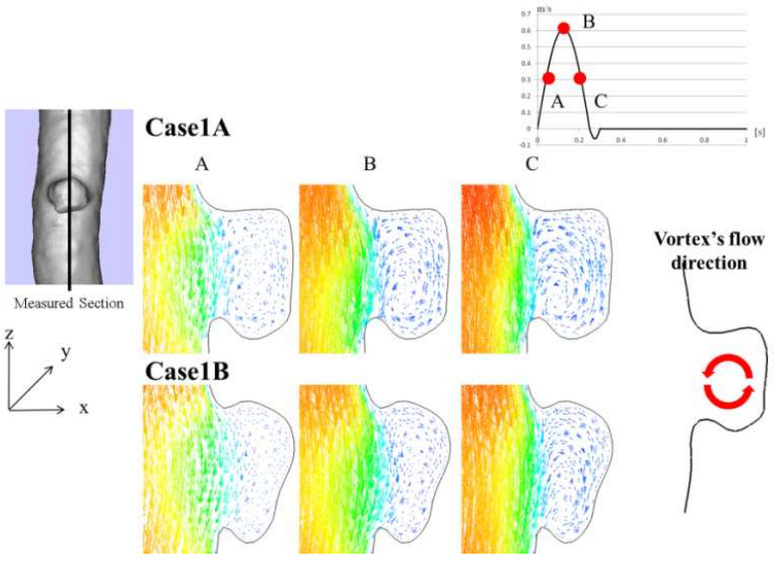

Figure 9. Secondary flow using the vectors in the horizontal sections for Case 1A (upper) and Case 1B (lower) at three time points (t=0.06, 0.12, and 0.18); the direction of the vortex flow is illustrated using the vector at the right side.

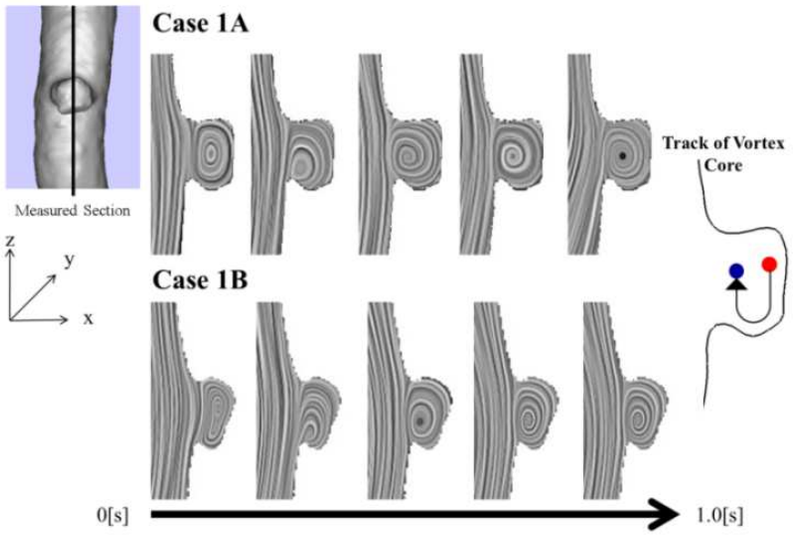

Figure 10. Movement of the vortex core using the LIC method for Case 1A (upper) and Case 1B (lower). For the track of the vortex core illustrated at the right side,the red point is the start point and the blue point is the end point.

Figure 11 shows the pressure distributions using the contours for each case at four time points. The pressure distribution values were set in the range where the ULP was emphasized. At A (t=0.06), the pressure distribution had its maximum value for the entire ULP. At the bottom side of the ULP, the pressure distribution was higher than that at other parts. Figure 12 shows the pressure distributions for each case at four time points. These four points were decided by observing the formation in Case 1B. The pressure distributions at p2, p3, and p4 were higher than at p1. When the ULP was observed in Case 1A, the progression of the configuration was observed in the high pressure region. During the progression in Case 1B, a similar trend was seen. For Case 1B, the ULP had the possibility of rupturing, which corresponded with the diagnosis made by the doctor.

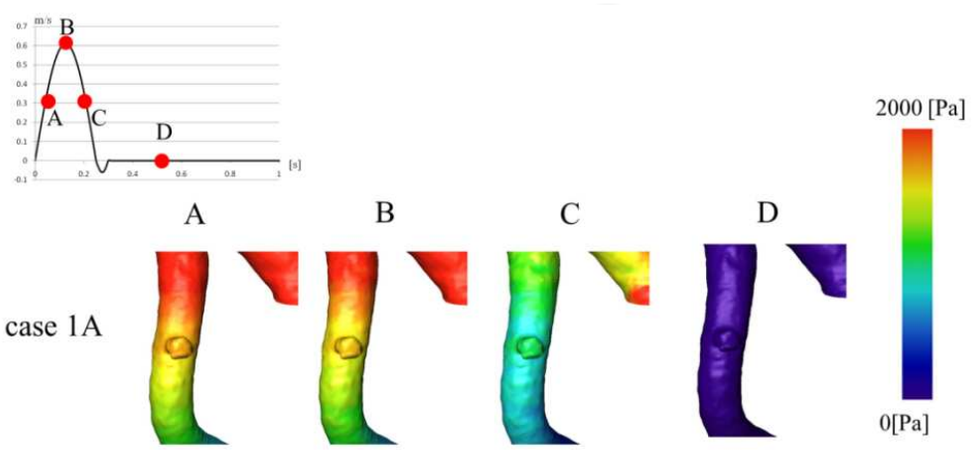

Figure 11. Pressure distributions in Case 1A at four time points. The pressure distribution values were set in the range where the ULP was emphasized.

http://dx.doi.org/10.5772/52559

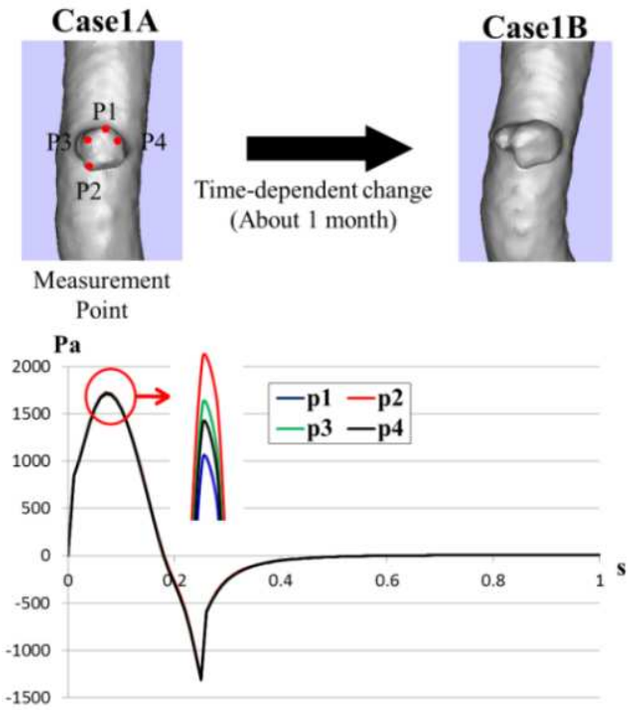

Figure 12. Pressure distributions at four time points for the ULP in Case 1A. The X axis indicatestime and the Y axis indicates the pressure distribution. Blue indicates p1 values, red indicates p2 values, green indicates p3 values, and black indicates p4 values.

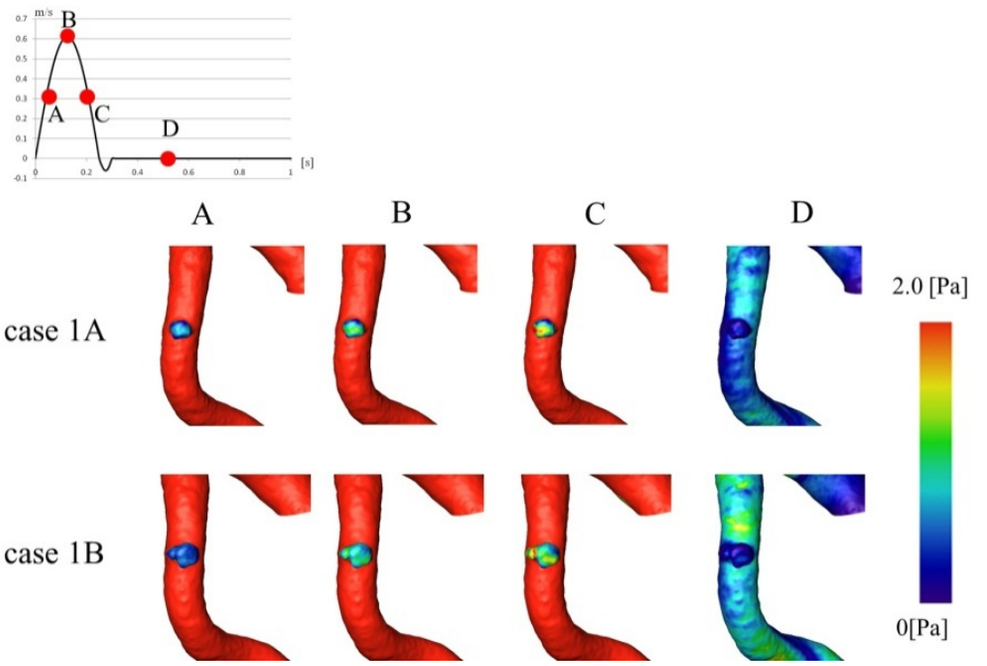

Figure 13. WSS distributionsin Case 1A and Case 1B at four time points (t=0.06, 0.12, 018, and 0.50) using their contours. The WSS distribution values were set in the range where the ULP was emphasized.

Figure 13 shows the WSS distributionsfor Case 1A and Case 1B using contours. The WSS distribution valueswere set in the range where the ULP was emphasized. At C (t=0.18), a high WSS is seen at the left side. Figure 14 shows WSS distributions in each case at four time points. The WSS distributionsat p2, p3, and p4 were lower than that at p1. When the ULP in case1A was observed, the progression of the configuration was observed in the low WSS distribution region. During the progression for Case 1B, a similar trend was seen. These results are in agreement with the results of Sheidaei [36, 37] which indicate that the region of higher expansion correlates with regions of a low WSS. Figure 15 shows the direction of WSSvectors at p2, p3, and p4. In Case 1A, the vortexes was observed at p3 and p4, and the direction of WSS vectors was separated in p2. The change in the direction of WSS vectors was seen in the area that had progressed.

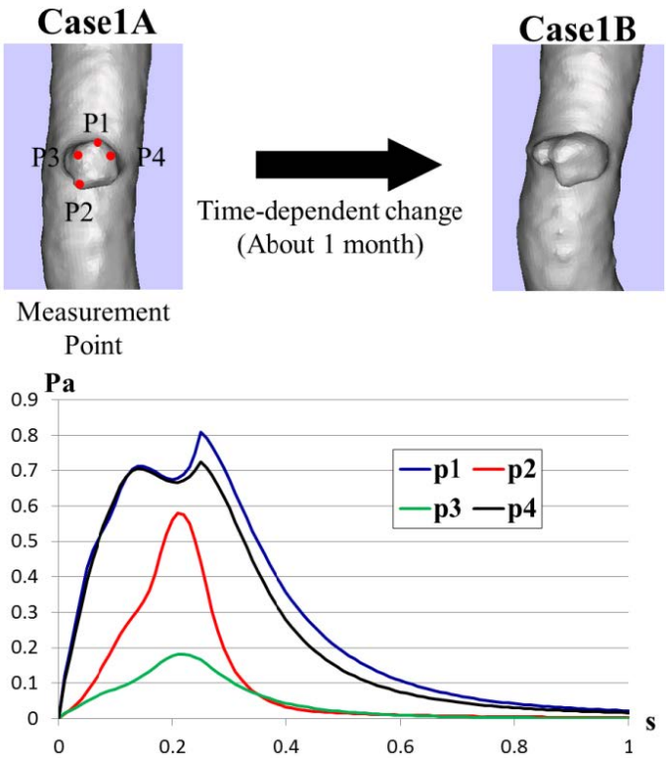

Figure 14. WSS distributions at four time points of the ULP in Case 1A. X axis indicates time and the Y axis indicates the WSS distribution. Blue indicates p1 values, red indicates p2 values, green indicates p3 values, and black indicates p4 values.

http://dx.doi.org/10.5772/52559

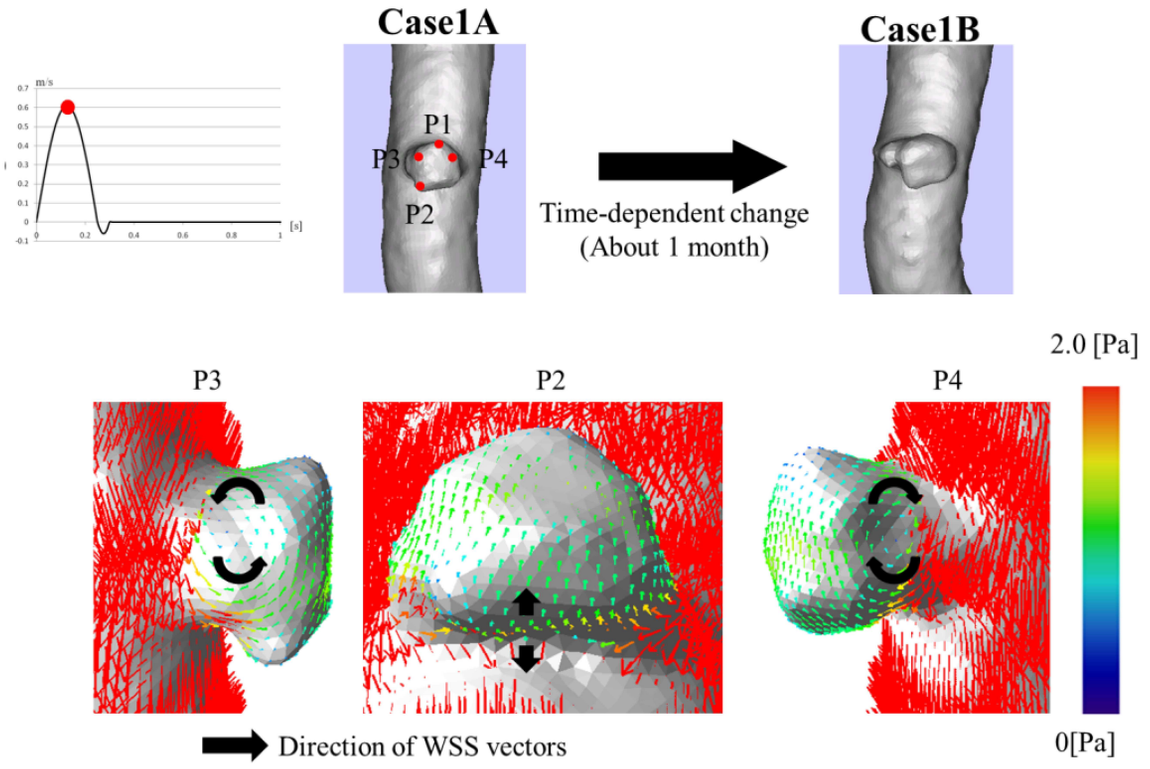

Figure 15. Direction of WSS vectors at the peak of velocity (t=0.12) using the vector. The color indicates the WSS distribution. The black arrow indicates the direction of WSS vectors. The WSS distribution values were set in the range where the ULP was emphasized.

4. Conclusions

We analyzed aortic dissections with ULPs of the complete thrombosis type using CFD simulations. In ULPs showed tendencies for expansion, the movement of the vortex cores exhibited similar tendencies. In addition, multiple vortexes were observed when a diagnosis of immediate rupture was made. Moreover, it was found that the high pressure and low WSS distribution were indictors of progression. The change in the direction of WSS vectors was seen in the area that had progressed.Thus, it is possible to predict the time-dependent change of the disease using CFD simulation.

The time-dependent change of the ULP becomes the standard of the diagnosis in aortic dissection. To examine the predictive hemodynamic factors for an ULP due to an aortic dissection of the complete thrombosis type, we reconstructed and analyzed a model blood vessel using time-series medical images. We identified the predictive hemodynamics factors. Valuable information can be obtained by combining a clinical diagnosis with fluid dynamics simulations.

Author details

Futoshi Mori[1,2,3], Hiroshi Ohtake[4], Go Watanabe[4] and Teruo Matsuzawa[5*]

*Address all correspondence to: f-mori@eri.u-tokyo.ac.jp

*Address all correspondence to: matuzawa@jaist.ac.jp

1 School of Information Science, Japan Advanced Institute of Science and Technology, Japan

2 Interfaculty Initiative in Information Studies, The University of Tokyo, Japan

3 Earthquake Research Institute, The University of Tokyo, Japan

4 Department of General and Cardiothoracic Surgery, Kanazawa University, Japan

5 Research Center for Simulation Science, Japan Advanced Institute of Science and Technology, Japan

References

[1] The Japanese Circulation Society. JCS. http://www.j-circ.or.jp/guideline/index.html/ (accessed 5August (2012).

[2] Hiratzka, L. F., Bakris, G. L., Beckman, J. A., Bersin, R. M., Carr, V. F., Casey, D. E., Jr , , Eagle, K. A., Hermann, L. K., Isselbacher, E. M., Kazerooni, E. A., Kouchoukos, N. T., Lytle, B. W., Milewicz, D. M., Reich, D. L., Sen, S., Shinn, J. A., Svensson, L. G., & Williams, D. M. 2010ACCF/AHA/AATS/ACR/ASA/SCA/SCAI/SIR/STS/SVM guidelines for the diagnosis and management of patients with thoracic aortic disease: executive summary. A report of the American College of Cardiology Foundation/ American Heart Association Task Force on Practice Guidelines, American Association for Thoracic Surgery, American College of Radiology, American Stroke Association, Society of Cardiovascular Anesthesiologists, Society for Cardiovascular Angiography and Interventions, Society of Interventional Radiology, Society of Thoracic Surgeons, and Society for Vascular Medicine. Circulation 2010;, 121, 1544-1579.

[3] Roberts WC. Aortic dissection: anatomy, consequences, and cause.American heart journal (1981). , 101, 195-214.

[4] Information for Patients from the International Registry of Acute Aortic Dissection.http://www.iradonline.org/about.htmlaccessed 5 August (2012).

[5] Daily, P. O., Trueblood, H. W., Stinson, E. B., Wuerflein, R. D., & Shumway, N. E. (1970). Management of acute aortic dissections. *The Annals of thoracic surgery*, 10, 237-247.

[6] Debakey, , Henly, W. S., Cooley, D. A., Morris, G. C., Jr , , Crawford, E. S., Beall, A. C., & Jr , . Surgical Management of Dissecting Aneurysms of the Aorta. The Journal of thoracic and cardiovascular surgery (1965). , 49, 130-149.

[7] Tsai, T. T., Evangelista, A., Nienaber, , Myrmel, T., Meinhardt, G., Cooper, J. V., Smith, D. E., Suzuki, T., Fattori, R., Llovet, A., Froehlich, J., Hutchison, S., Distante, A., Sundt, T., Beckman, J., Januzzi, J. L., Jr , , Isselbacher, E. M., & Eagle, K. A. Partial Thrombosis of the False Lumen in Patients with Acute Type B Aortic Dissection. The New England Journal of Medicine (2007). , 357, 349-359.

[8] Nienaber, , von, Kodolitsch. Y., Petersen, B., Loose, R., Helmchen, U., Haverich, A., & Spielmann, R. P. Intramural hemorrhage of the thoracic aorta. Diagnostic and therapeutic implications. Circulation (1995). , 92, 1465-1472.

[9] Aortic Dissection- Cedars-Sinai. http://www.cedars-sinai.edu/Patients/Health-Conditions/Aortic-Dissection.aspx (accessed 5August (2012).

[10] Stanson, A. W., Kazmier, F. J., Hollier, L. H., Edwards, W. D., Pairolero, P. C., Sheedy, P. F., Joyce, J. W., & Johnson, M. C. (1986). Penetrating atherosclerotic ulcers of the thoracic aorta: natural history and clinicopathologic correlations. *Annals of Vascular Surgery*, 1, 15-23.

[11] Hayashi, H., Matsuoka, Y., Sakamoto, I., Sueyoshi, E., Okimoto, T., Hayashi, K., & Matsunaga, N. Penetrating Atherosclerotic Ulcer of the Aorta: Imaging Features and Disease Concept. Radiographics (2000). , 20, 995-1005.

[12] Wu, M. T., Wang, Y. C., Huang, Y. L., Chang, R. S., Li, S. C., Yang, P., Wu, T. H., Chiou, K. R., Huang, J. S., Liang, H. L., & Pan, H. B. (2011). Intramural blood pools accompanying aortic intramural hematoma: CT appearance and natural course. *Radiology*, 258, 705-713.

[13] Park, G. M., Ahn, J. M., Kim, D. H., Kang, J. W., Song, J. M., Kang, D. H., Lim, T. H., & Song, J. K. (2011). Distal aortic intramural hematoma: clinical importance of focal contrast enhancement on CT images. *Radiology*, 259, 100-108.

[14] Kitai, T., Kaji, S., Yamamuro, A., Tani, T., Kinoshita, M., Ehara, N., Kobori, A., Kita, T., & Furukawa, Y. Impact of New Development of Ulcer-Like Projection on Clinical Outcomes in Patients With Type B Aortic Dissection With Closed and Thrombosed False Lumen. Circulation (2010). SS80., 74.

[15] Kitai, T., Kaji, S., Yamamuro, A., Tani, T., Kinoshita, M., Ehara, N., Kobori, A., Kim, K., Kita, T., & Furukawa, Y. Detection of intimal defect by 64 -row multidetector computed tomography in patients with acute aortic intramural hematoma. Circulation(2011). S174-S178.

[16] Ganaha, F., Miller, D. C., Sugimoto, K., , Y. S., Minamiguchi, H., Saito, H., Mitchell, R. S., & Dake, . Prognosis of aortic intramural hematoma with and without penetrating atherosclerotic ulcer. Circulation (2002). ; ., 106, 342-348.

[17] Sueyoshi, E., Matsuoka, Y., Sakamoto, I., Uetani, M., Kuniaki, H., & Narimatsu, M. (1997). Fate of intramural hematoma of the aorta: CT evaluation. *Journal of computer assisted tomography*, 21, 931-938.

[18] Moizumi, Y., Komatsu, T., Motoyoshi, N., & Tabayashi, K. (2004). Clinical features and long-term outcome of type A and type B intramural hematoma of the aorta. *The Journal of thoracic and cardiovascular surgery*, 127, 421-427.

[19] Enlargement of ulcer-like projections after repair of acute type A aortic dissection. The Annals of thoracic surgery; ., 68, 1860-1863.

[20] Jang, Y. M., Seo, J. B., Lee, Y. K., Chae, E. J., Park, S. H., Kang, J. W., & Lim, T. H. Newly developed ulcer-like projection (ULP) in aortic intramural haematoma on follow-up CT: is it different from the ULP seen on the initial CT?. Clinical Radiology (2008). , 63, 201-206.

[21] Kaji, S., Akasaka, T., Katayama, M., Yamabe, K., Tamita, K., Akiyama, M., Watanabe, N., Tanemoto, K., Morioka, S., & Yoshida, K. Long-term prognosis of patients with type B aortic intramural hematoma. Circulation(2003). IIII311., 307.

[22] Kawamata, H., & Kumazaki, T. Ulcerlike Projections of the Thrombosed Type Aortic Dissection- Their Incidence, Locations and Natural History-. The Journal of Japanese College of Angiology (1994). , 34, 1017-1032.

[23] Fukushima, T., Matsuzawa, T., & Homma, T. (1989). Visualization and finite element analysis of pulsatile flow in models of the abdominal aortic aneurysm. *Biorheology*, 26, 109-130.

[24] Boecher-Schwarz, H. G., Ringel, K., Kopacz, L., Heimann, A., & Kempski, O. Ex vivo study of the physical effect of coils on pressure and flow dynamics in experimental aneurysms. American Journal of Neuroradiology (2000). , 21, 1532-36.

[25] Metcalfe RW.The promise of computational fluid dynamics as a tool for delineating therapeutic options in the treatment of aneurysms. American Jounal of Neuroradiology (2003). , 24, 553-554.

[26] Boussel, L., Rayz, V., Mc Culloch, C., Martin, A., Acevedo-Bolton, G., Lawton, M., Higashida, R., Smith, W. S., Young, W. L., & Saloner, D. Aneurysm growth occurs at region of low wall shear stress patient-specificcorrelation of hemodynamics and growth in a longitudinal study. Stroke(2008). , 39, 2997-3002.

[27] Bluestein, D., Niu, L., Schoephoerster, R. T., & Dewanjee, M. K. Steady flow in ananeurysm model: correlation between fluid dynamics and blood plateletdeposition. Journal of Biomechanical Engineering-Transactions of the ASME(1996). , 118, 280-286.

[28] Shojima, M., Oshima, M., Takagi, K., Torii, R., Hayakawa, M., Katada, K., Morita, A., & Kirino, T. Magnitudeand role of wall shear stress on cerebral aneurysm-computationalfluid dynamic study of 20 middle cerebral artery aneurysms. Stroke(2004). , 35, 2500-2505.

[29] Valencia, A., Morales, H., Rivera, R., Bravo, E., & Galvez, M. Blood flow dynamicsin patient-specific cerebral aneurysm models: The relationship betweenwall shear stress and aneurysm area index. Medical Engineering & Physics(2008). , 30, 329-340.

[30] Karmonik, C., Bismuth, J., Shah, D. J., Davies, M. G., Purdy, D., & Lumsden, A. B. Computational Study of Haemodynamic Effects of Entry- and Exit-Tear Coverage in a DeBakey Type III Aortic Dissection: Technical Report. European journal of vascular and endovascular surgery (2011). , 42, 172-177.

[31] Watanabe, M., & Matsuzawa, T. (2006). Unsteady and three-dimensional simulation of blood flow in aortic dissection reconstructed from CT images. *Journal of Biomechanics*, S294 EOF.

[32] Shimogoya, Y., Ishikawa, T., Imai, Y., Matsuki, T., Yamaguchi, T. A., realistic, simulation., of, saccular., cerebral, aneurysm., formation, focusing., on, a., novel, hemodynamic., index, the., gradient, oscillatory., & number, . G. O. N. International Journal of Computational Fluid Dynamic (2009). , 8, 583-593.

[33] Stein PD., and Sabbah HN. (1976). Turbulent blood flow in the ascending aorta of humans with normal and diseased aortic valves. *Circulation research*, 39, 58-65.

[34] Fu, W., Chu, B., Chang, Yu., & Qiao, A. Construction and Analysis of Human Thoracic Aorta Based on CT Images. IFMBE Proceeding (2010). , 25, 322-325.

[35] Xiang, J., Natarajan, S. K., Tremmel, M., , D., Mocco, J., Hopkins, L. N., Siddiqui, A. H., Levy, E. L., Meng, H., & Hemodynamic, . Hemodynamic-Morphologic Discriminants for Intracranial Aneurysm Rupture. Stroke (2011). , 42, 144-152.

[36] Tremmel, M., Dhar, S., Levy, E. I., Mocco, J., & Meng, H. (2009). Influence of intracranial aneurysm-to-parent vessel size ratio on hemodynamics and implication for rupture: results from a virtual experimental study. *Neurosurgery*, 64, 622-630.

[37] Shidaei, A., Hunley, S. C., Zeinali-Davarani, S., Raguin, L. G., & Baek, S. Simulation of abdominal aortic aneurysm growth with updating hemodynamic loads using a realistic geometry. Medical Engineering & Physics (2011). , 33, 80-88.

IntechOpen